ACS Catalysis

Research Article

pubs.acs.org/acscatalysis

Periodic Trends in Highly Dispersed Groups IV and V Supported Metal Oxide Catalysts for Alkene Epoxidation with H_2O_2

Nicholas E. Thornburg, Anthony B. Thompson, and Justin M. Notestein*

Department of Chemical and Biological Engineering, Technological Institute E136, Northwestern University, 2145 Sheridan Road, Evanston, Illinois 60208, United States

Supporting Information

ABSTRACT: Supported metal oxides are important catalysts for selective oxidation processes like alkene epoxidation with H_2O_2. The reactivity of these catalysts is dependent on both identity and oxide structure. The dependence of the latter on the synthesis method can confound attempts at comparative studies across the periodic table. Here, SiO_2-supported metal oxide catalysts of Ti(IV), Zr(IV), Hf(IV), V(V), Nb(V), and Ta(V) (all of groups IV and V) were synthesized by grafting a series of related calixarene coordination complexes at surface densities less than ~0.25 nm^{-2}. Select catalysts were investigated by solid state NMR, UV−visible, and X-ray absorption near-edge spectroscopies. As-synthesized and calcined materials were examined for the epoxidation of cyclohexene and styrene (1.0 M) with H_2O_2 (0.10 M) at 45 and 65 °C. Nb catalysts emerge as high-performing materials, with calcined Nb−SiO_2 proceeding at a cyclohexene turnover frequency of 2.4 min^{-1} (>2 times faster than Ti−SiO_2) and with ~85% selectivity toward direct (nonradical) epoxidation pathways. As-synthesized Zr, Hf, and Ta catalysts have improved direct pathway selectivities compared with their calcined versions, particularly evident for Ta−SiO_2. Finally, when the materials are synthesized from these precursors but not simple metal chlorides, the direct pathway reaction rate correlates with Pauling electronegativities of the metals, demonstrating clear periodic trends in intrinsic Lewis acid catalytic behavior.

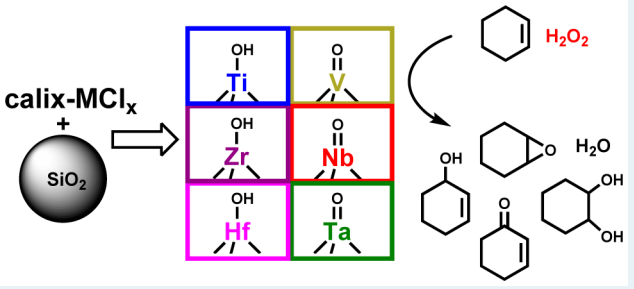

KEYWORDS: *supported catalyst, supported oxide, niobium, calixarene, olefin epoxidation, hydrogen peroxide, green chemistry*

INTRODUCTION

Supported metal oxide catalysts are ubiquitous in both commodity and fine chemical manufacturing, particularly for selective oxidations of alkanes, alkenes, alcohols, and aromatics, as well as oxidative dehydrogenation, hydroxylation, and ammoxidation.[1−3] Separately, alkene epoxidation is widely studied for organic synthesis, and there is a desire to use supported metal oxide catalysts with H_2O_2 instead of alkyl hydroperoxides. H_2O_2 is environmentally advantageous, and its process economics are not dependent on selling or disposing of a coproduct.[4,5]

Ti(IV) oxide on SiO_2 (Ti−SiO_2) is a benchmark Lewis acid catalyst for epoxidation with organic hydroperoxides, whereas Ti embedded in a silicate framework (e.g., TS-1) is preferred for H_2O_2.[2,6−11] It is accepted that tetrahedrally coordinated Ti sites are the most reactive and selective for epoxidation with hydroperoxides,[6,7,12−14] so synthesis methods are designed to give the high dispersions on SiO_2 that result in a preponderance of such sites.[14−17] For example, grafting bulky molecular precursors leads to more active and selective catalysts on a per-Ti basis.[9,10,14,15,17]

Aside from Ti−SiO_2, Ta(V)[18−21] and Nb(V)[22−27] oxides on SiO_2 (Ta−SiO_2 and Nb−SiO_2) have demonstrated high selectivity, activity, and stability for epoxidation with aqueous H_2O_2 oxidant, but in fewer reports. The extra anionic coordination site of Ta oxides has been suggested to be responsible for their higher water tolerance and faster turnover in the presence of water relative to Ti−SiO_2.[19−21] Vanadium(V) oxides on SiO_2 (V−SiO_2) are well-studied for oxidation,[28,29] but they are poorly selective epoxidation catalysts[23] believed to operate via oxovanadium intermediates rather than through peroxymetal species such as for Ti−SiO_2, Ta−SiO_2, and Nb−SiO_2.[4,30,31] Grafted Zr(IV) catalysts (Zr−SiO_2) have not been reported for epoxidation, to our knowledge, but in-framework Zr-beta materials[32,33] and Zr-containing polyoxometalates[34] show poor activity and selectivity for epoxidation compared with analogous Ti materials. Finally, to our knowledge, supported Hf(IV) catalysts (Hf−SiO_2) have not been reported for epoxidation, although homogeneous studies show selectivities similar to those of Ti analogues.[35−37]

Beyond individual catalyst studies, there are few head-to-head comparisons of different supported metal oxides for epoxidation. In the 70s, Sheldon benchmarked several homogeneous and SiO_2-supported catalysts for olefin epoxidation with alkyl hydroperoxides and found high activity and selectivity with Ti(IV) and Mo(VI), the latter of which poorly performed when

Received: May 26, 2015
Revised: July 21, 2015
Published: July 22, 2015

DOI: 10.1021/acscatal.5b01105
ACS Catal. 2015, 5, 5077−5088

Scheme 1. Synthesis of Group IV and V Calixarene Complexes, Their Grafting onto SiO_2, and Subsequent Calcination To Yield Highly Dispersed Metal Oxides[a]

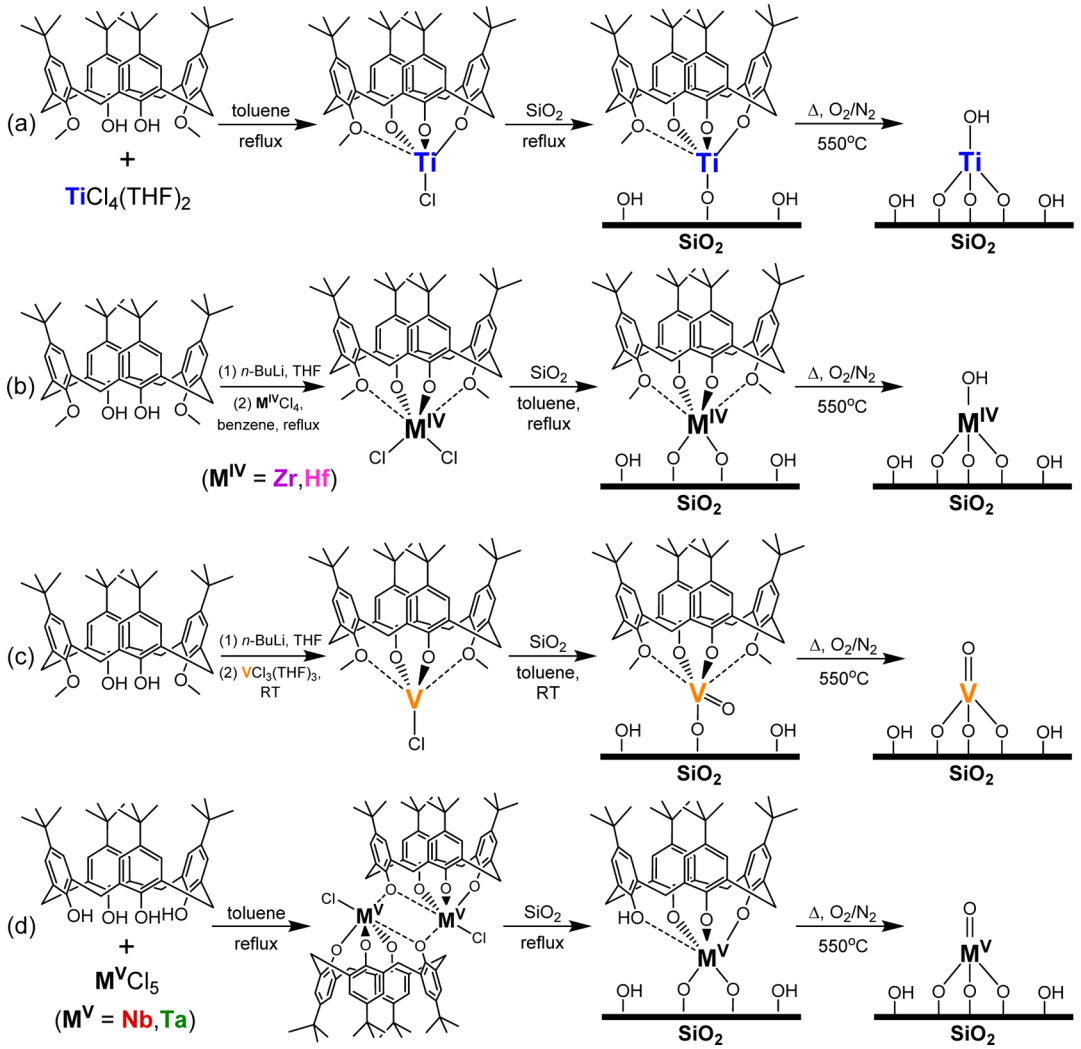

[a](a) for Ti, (b) for Zr and Hf, (c) for V, and (d) for Nb and Ta. Full details of synthetic procedures are included in the Supporting Information.

supported due to significant leaching.[4,30] Because supported metal oxide structure (e.g., extent of M−O−M vs M−O−Si bonding) plays a strong role in its epoxidation reactivity,[8,10,11,17,26,38,39] cross-comparisons among related metal oxides may become confounded if differences in the synthesis method or precursor lead to a variation in surface oxide species. Therefore, here, we graft well-defined calixarene coordination complexes of groups IV and V onto SiO_2 to create a structurally uniform set of catalysts for comparison in epoxidation with H_2O_2. The calixarene ligand is bulky and strongly chelated to the metal, which some of us have shown to give under-coordinated, highly active Ti−SiO_2[40−42] and Ta−SiO_2[21] epoxidation catalysts. Here, we broaden this strategy to the rest of groups IV and V to draw correlations for Lewis acid-catalyzed epoxidation over a large family of supported oxides.

EXPERIMENTAL METHODS

Catalyst Synthesis. All catalyst syntheses were performed using standard Schlenk line techniques under N_2 or in a controlled Ar atmosphere glovebox. Solvents (toluene, tetrahydrofuran, benzene, *n*-hexane) were distilled and degasified by standard methods and stored inside the glovebox. $TiCl_4(THF)_2$, $ZrCl_4(THF)_2$, $HfCl_4$, $VCl_3(THF)_3$, $NbCl_5$, and $TaCl_5$ were used as received from Strem Chemicals and stored inside the glovebox. p-*tert*-Butylcalix[4]arene (95%) ("Calix") was used as received from Sigma-Aldrich. 1,3-Dimethoxy-*tert*-butylcalix[4]arene ("dmCalix") was prepared according to a published procedure.[43] Calixarene coordination complexes were prepared by reacting stoichiometric metal chloride and calixarene ligand, generally following known procedures described below. Synthesis was followed by isolation or direct grafting onto SiO_2 (Selecto Scientific, 32−62 μm particle size, 570 $m^2\ g^{-1}$, 5.4 nm avg. pore dia.) that had been partially dehydroxylated at 300 °C under dynamic vacuum (<50 mTorr) for 10 h (Scheme 1). Following grafting, all dry solids were sieved to ≤88 μm particle size. See Supporting Information for full syntheses, NMR resonances, and elemental analyses.

For complexes of Ti, Nb, and Ta, dmCalix (Ti) or Calix (Nb, Ta) and stoichiometric metal chloride were refluxed in toluene with a N_2 sparge until HCl evolution ceased, giving the monomethoxycalixarene complex (mmCalix−TiCl)[44] or the associated dimers of the Calix−NbCl[45] and Calix−TaCl[46] complexes. Complexes were isolated by solvent removal via rotary evaporation and trituration with *n*-hexane. The calixarene

DOI: 10.1021/acscatal.5b01105
ACS Catal. 2015, 5, 5077−5088

complexes were grafted to SiO_2 from refluxing toluene. After reaction, the solids were washed in toluene, Soxhlet extracted in toluene, and dried under dynamic vacuum. Some of us have previously reported SiO_2 grafting of the Ti[40] and Ta[21] complexes to give bright orange solids.

For complexes of Zr,[47] Hf, and V,[48,49] dmCalix was suspended in THF, reacted with 2 equiv of *n*-butyllithium (1.6 M in hexanes; Sigma), and added dropwise to the metal chloride solutions in benzene (Zr, Hf) or THF (V). The solvent was removed by rotary evaporation, and residues were extracted into 5:1 anhydrous *n*-hexane/benzene. The isolated calixarene complexes were redissolved in toluene inside a glovebox and subsequently grafted to SiO_2. Following grafting, solids were washed with toluene, THF (Zr, Hf) or *n*-hexane (V), and water before drying under dynamic vacuum.

As-synthesized Calix−M−SiO_2 (M = Ti, Zr, Hf, V, Nb, Ta) catalysts were heated in air at a ramp of 10 °C min^{-1} and held at 550 °C for 6 h to remove organic content and give M−SiO_2. A control Nb-containing catalyst was synthesized by refluxing $NbCl_5$ and SiO_2 in toluene for 24 h with continuous sparging of N_2. The final suspension was vacuum-filtered, washed with toluene, dried under dynamic vacuum, and calcined as above to give $NbCl_5$−SiO_2.

Characterization. Metal content was quantified using inductively coupled plasma atomic emission spectroscopy (ICP−AES; Varian Vista MPX) calibrated against serial dilution of commercial standard solutions (Fluka Analytical) in 0.9 wt % HNO_3. Catalysts were digested in 48 wt % HF and diluted with 0.9 wt % HNO_3. [CAUTION: Handle and store HF with extreme care.] Multiple trials were averaged. C and H contents of calixarene complexes were determined by combustion analysis (Galbraith Laboratories, Knoxville, TN).

Thermogravimetric analysis (TGA; TA Instruments Q500) of as-synthesized catalysts was carried out under dry synthetic air (90% O_2, 10% N_2, 100 mL min^{-1}) at a ramp of 10 °C min^{-1} from room temperature to 800 °C and compared with mass loss by bare SiO_2 to correct for support hydroxyl condenstation. Calixarene content was estimated by assuming combustion of ligands with molecular weight 629 g mol^{-1} (mmCalix−Ti), 643 g mol^{-1} (dmCalix−Zr, −Hf, and −V), or 613 g mol^{-1} (Calix−Nb and −Ta). Surface densities are reported relative to the N_2 physisorption surface area (Micromeritics ASAP 2010 CE system) of the unmodified, dehydroxylated support.

UV−visible spectra of solids were measured from 700 to 200 nm at ambient conditions using a Shimadzu UV-3600 and a Harrick Praying Mantis diffuse reflectance accessory (DRUV−vis). Polytetrafluoroethylene powder was used to collect a "perfect" reflectance baseline for Kubelka−Munk pseudoabsorbances and as a 20:1 diluent for catalyst samples. Optical edge energies were computed from the *x*-intercept of the indirect Tauc plot of $[F(R)\cdot h\nu]^{1/2}$ vs $h\nu$ (eV), where $F(R)$ is the Kubelka−Munk pseudoabsorbance. UV−visible spectra of some calixarene complexes were collected in acetonitrile solution and a 1 cm path length quartz cell over the same wavelength range (Figure S1). Solution-phase ^1H NMR and ^{13}C NMR spectra of these complexes were obtained on a Bruker Avance III 500 MHz spectrometer with direct cryoprobe. Solid state ^{13}C cross-polarization magic angle spinning (CP−MAS) NMR spectra were collected on a 400 MHz Varian spectrometer at a spin rate of 5 kHz.

X-ray absorption near-edge spectroscopy (XANES) was performed at the Ti K-edge (4966.4 eV), the V K-edge (5465.1 eV), the Nb K-edge (18 985.6 eV), and the Ta L_3-edge (9881.1 eV) using bending magnet station D at the Advanced Photon Source beamline at Sector 5 (DuPont−Northwestern−Dow Collaborative Access Team (DND-CAT)) of Argonne National Laboratory. The beam energy was controlled using a Si(111) monochromator with 10^{-4} eV resolution. Beam energies and detectors were calibrated to the above edges using pure metal foil in transmission mode. Standards were brushed onto Kapton tape, and spectra were collected at ambient conditions in transmission mode. V_2O_5, Nb_2O_5, and Ta_2O_5 standards were used as received from Strem Chemicals. Anatase TiO_2 was uses as received from Sigma-Aldrich. $KNbO_3$ was used as received from Alfa Aesar. Ba_2TiO_4 was prepared according to a literature procedure.[50] $YNbO_4$ and $CaNb_2O_6$ and were prepared according to slightly modified literature procedures (see Supporting Information).[51,52] Powder X-ray diffraction patterns of $YNbO_4$ and $CaNb_2O_6$ were obtained using a Rigaku Ultima IV diffractometer with Cu K_α radiation, a step width of 0.1°, and a receiving slit size of 0.6 nm and verified using the pattern-matching features of the MDI Jade 2010 analysis software (Figure S2). Fresnoite ($Ba_2(TiO)Si_2O_7$) was provided by the E. Bruce Watson Research Group at the Rensselaer Polytechnic Institute. Catalyst samples were analyzed in fluorescence mode by using a four-channel Canberra SII Vortex ME4 detector with a controlled atmosphere sample cell oriented at 45° ± 5° to the detector and to the incident X-ray beam. Catalysts were loaded into a sealed controlled atmosphere cell, evacuated to −20 inHg gauge, heated under dynamic vacuum at 150 °C for 2 h, and sealed under purified Ar prior to spectroscopy.

Catalysis. Cyclohexene (>99%, Sigma) and styrene (>99%, Sigma) were passed over a column of activated Alumina N (Selecto Scientific, 63−150 μm) immediately before use. A 4.0 M solution of H_2O_2 in acetonitrile was prepared by diluting 10 mL aqueous H_2O_2 (30% w/w) in 20 mL acetonitrile, followed by drying with 7.0 g anhydrous $MgSO_4$ (>99%, Sigma) and decanting. H_2O_2 concentration was quantified using permanganimetric titration.

Epoxidation was performed in 20 mL septum-cap glass vials vented with a needle. In a typical experiment, 10.9 mmol of alkene, 0.01 mmol of metal (60−90 mg of solids) catalyst, and 1.30 mmol of 1,2-dichlorobenzene (98%, Alfa Aesar) internal standard were added to 9 mL of acetonitrile (>99%, spectrophotometric grade, Alfa Aesar), heated to 35−65 °C, and shaken at 700 rpm on a Glas-Col heated vortexer. For reactions at 75 °C, a 25 mL round-bottom flask equipped with a reflux condenser and a stirbar was used. The reaction was initiated with the instantaneous addition of 1.08 mmol of H_2O_2. This gives initial conditions of $[\text{cyclohexene or styrene}]_0$ = 1.02 M, $[H_2O_2]_0$ = 0.103 M, alkene/H_2O_2/M = 1000:100:1, and a total reaction volume of 10.4−10.6 mL. Reaction aliquots were passed through a Whatman 0.7 μm glass microfiber filter and contacted with Ag powder (>99%, < 250 μm, Sigma) to quench unreacted H_2O_2. Products from cyclohexene oxidation were identified by GC/MS (Shimadzu QP2010 GC/MS, Zebron ZB-624 capillary column) and quantified using GC−FID (Shimadzu 2010 GC−FID, TR-1 capillary column) against calibrated standards. Products from styrene oxidation were identified and quantified by GC/MS. In all kinetic experiments, mass balances were ≥85%.

Catalyst leaching was tested by running cyclohexene oxidation for 10−15 min at 65 °C, after which the shaking was stopped; the solids were allowed to settle; and the liquid contents were quickly transferred using a glass pasteur pipette (no filter) to a clean, heated 20 mL septum-cap vial, where the

DOI: 10.1021/acscatal.5b01105
ACS Catal. 2015, 5, 5077−5088

Table 1. Summary of Grafted Catalysts

		metal content[b]			
catalyst precursor	[Calix][a] (mmol g^{-1})	(mmol g^{-1})	(M nm^{-2})[c]	wt %	M/Calix
mmCalix–Ti	0.18	0.18	0.19	0.9	1.0
dmCalix–Zr	0.11	0.19	0.21	1.8	1.8
dmCalix–Hf	0.11	0.19	0.20	3.5	1.8
dmCalix–V	0.11	0.25	0.26	1.3	2.3
Calix–Nb	0.11	0.18	0.19	1.7	1.7
$NbCl_5$		0.19	0.19	1.8	
Calix–Ta	0.18	0.19	0.21	3.6	1.1

[a]From TGA combustion analysis of as-synthesized catalysts. [b]From ICP–AES of calcined catalysts. [c]Using the SiO_2 support BET specific surface area of 570 m^2 g^{-1}.

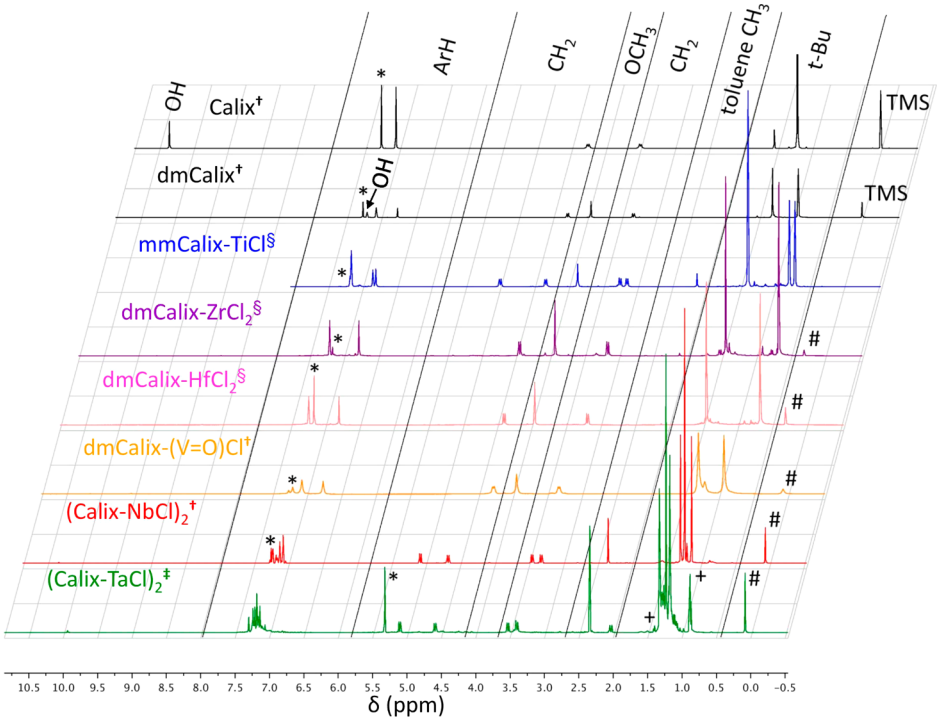

Figure 1. ^{1}H NMR spectra of calixarene complexes of groups IV and V and of their starting calixarenes. * = NMR solvent († = $CDCl_3$, § = C_6D_6, ‡ = CD_2Cl_2); TMS = tetramethylsilane (internal standard); + = residual *n*-hexane (from synthesis); # = vacuum grease.

reaction continued as usual. Some samples were transferred to vials also containing 100 mg of dehydroxylated SiO_2 and an additional 0.54 mmol H_2O_2 (half the amount added at t = 0). Some catalysts used in cyclohexene epoxidation at 65 °C were vacuum-filtered, washed with 50 mL acetonitrile, dried under dynamic vacuum, and reused. After washing, some used catalysts were also recalcined at 550 °C in air for 6 h before reuse.

RESULTS

Materials Synthesis and Characterization. Calix[4]-arene complexes of Ti(IV), Zr(IV), Hf(IV), V(III), Nb(V), and Ta(V) were synthesized in accordance with literature or with analogy to known complexes in the case of Hf. Elemental analyses (see Supporting Information) indicate that the Ti, Nb, and Ta complexes strongly retain ∼1 molecule of toluene solvent, with no evidence of uncomplexed metal chloride. The complexes of Zr, Hf, and V contain ∼10% uncomplexed metal chloride and retain the LiCl coproduct. However, the final water washing of the grafted catalyst removes residual LiCl to <0.006 mmol g^{-1} (Li/M < 3%) as determined by ICP–AES. Metal content in the calcined catalysts and ligand content in the as-synthesized catalysts were determined using ICP–AES and TGA, respectively, and are reported in Table 1.

Catalyst syntheses used 0.3–0.5 complexes per nm^2 of added SiO_2, but the final metal surface densities are between 0.19 and 0.26 M nm^{-2}, consistent with a previously observed geometric maximum for grafting of these bulky complexes[40] and suggesting that the metal–calixarene complex is intact during synthesis. The control Nb–SiO_2 catalyst from $NbCl_5$ was synthesized to match these surface densities; it grafts quantitatively under these conditions. For Ti and Ta, metal/calixarene ratios in the as-synthesized catalysts are ∼1, indicating that the complex is stable on the surface. Ratios are higher for other metals, indicating that the ligand can be lost during postsynthesis washing steps. In particular, the Zr, Hf, and V-containing materials were extensively washed with water to remove residual LiCl, which may contribute to ligand loss. X-ray absorption near-edge spectroscopy (XANES) of the Ti,[9,14,53] V,[54,55] Nb,[39,54−58] and Ta[59,60] materials gave edge energies within 1 eV of standards for each metal's highest oxidation state, as expected (Table S1). This does confirm that

DOI: 10.1021/acscatal.5b01105
ACS Catal. 2015, 5, 5077−5088

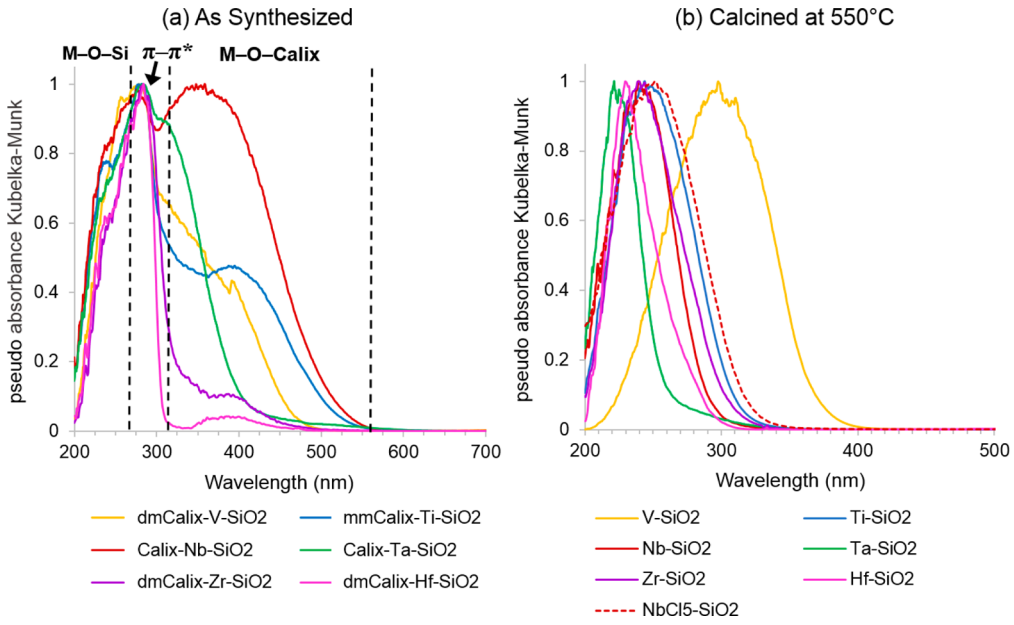

Figure 2. Diffuse reflectance UV−visible spectra for (a) as-synthesized materials, normalized to the $\pi-\pi^*$ transitions, and (b) calcined materials, normalized to the sole intense feature.

the V^{3+} precursor oxidized to V^{5+} after grafting, as intended. Additional discussion of the surface speciation of Ti and Nb catalysts is found in the Oxide Structure and Stability section.

Solution ^{1}H NMR spectra of the calixarene−metal complexes (Figure 1) do not show the OH resonances associated with the free ligands, and the diagnostic bridging methylene resonances are all shifted from that of the free ligand and are appropriate for the expected symmetry of the complexes.[61−63] Comparing the solid-state ^{13}C CP−MAS NMR spectra of the as-synthesized catalysts with the corresponding solution spectra of the precursors (Figure S3) shows diagnostic downfield shifts in the ipso carbons,[21] indicating calixarene−metal connectivity even when supported.

Peaks and optical edge energies from DRUV−vis spectroscopy provide insight into the metal oxide surface speciation.[8,14,64−67] Figure 2 shows the calixarene phenolate ligand-to-metal charge transfer band (LMCT) from 560 to 320 nm; aromatic $\pi-\pi^*$ transitions near 285 nm; and LMCT from support oxygens, typically near 250 nm. Normalized to the $\pi-\pi^*$ transition, the calixarene phenolate LMCT intensity varies dramatically from metal to metal in the general order Nb > Ti ∼ V > Ta > Zr > Hf. The Ta LMCT also appears to be shifted to higher energies than for the other materials.

After calcination (Figure 2b), the materials absorb only in the UV, evidence of highly dispersed metal oxide clusters. Optical edge energies from the indirect Tauc plot[14,64,65,68] are compared with literature values in Table 2. These high edge energies are consistent with prior values reported in the literature for grafted calixarenes and other precursors. Although edge energies have not been previously reported for analogous Zr−SiO_2 and Hf−SiO_2, optical edges and peak maxima estimated from published DRUV−vis of Zr-beta and Hf-beta[69] are consistent with those of our materials. Although the 3.1 eV edge of V−SiO_2 is lower than the other supported oxides, the value is consistent with energies reported by others.[49,70] The Ta−SiO_2 spectrum features a shoulder with an edge of 3.4 eV, suggesting some aggregation for this material. Crucially, the control Nb−SiO_2 from $NbCl_5$ has an edge energy

Table 2. Optical Edge Energies of Calcined Materials

catalyst	edge (eV)	literature edge (eV)	max (nm)
Ti−SiO_2	3.8	4.1[71]	244
Zr−SiO_2	3.7	3.9[69]	239
Hf−SiO_2	4.2	4.1[69]	230
V−SiO_2	3.1	3.2[70]	298
Nb−SiO_2	4.0	4.1[72]	240
$NbCl_5$−SiO_2	3.6	4.1[72]	252
Ta−SiO_2	3.4[a]; 4.5	4.8[21]	222

[a]Shoulder feature.

0.4 eV lower than Nb−SiO_2 from grafted calixarene−Nb, indicating that the grafted calixarene−Nb leads to more highly dispersed NbO_x structures than grafted $NbCl_5$ at equivalent metal loadings.

Cyclohexene Epoxidation. Following reaction networks proposed for TiO_x−SiO_2 systems,[73,74] cyclohexene epoxidation may occur via nonradical heterolytic activation of H_2O_2 ("direct") and along radical pathways via cyclohexenyl hydroperoxides in parallel (Scheme 2). Other reactions include

Scheme 2. Proposed Reaction Network for Cyclohexene Oxidation[21,73,74]

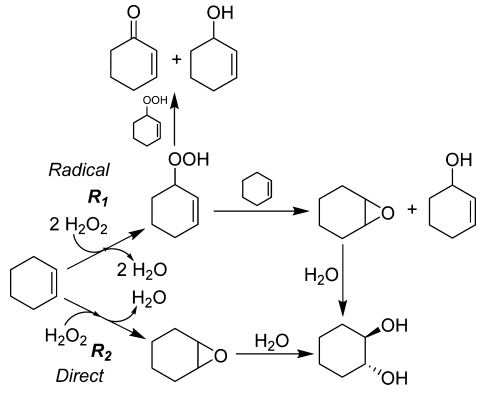

DOI: 10.1021/acscatal.5b01105
ACS Catal. 2015, 5, 5077−5088

Table 3. Selected Data for Cyclohexene Epoxidation by Calix−Ta−SiO_2 and Ta−SiO_2[a]

		initial TOF (mol mol_{Ta}^{-1} min^{-1})			6-h selectivity (%)			
catalyst	temp (°C)	total	direct	6-h yield (%)	epox	diol	other[b]	pathway sel. at ~25% yield (%)
Calix−Ta−SiO_2	35	0.79	0.77	58	73	26	1	97
	45	0.99	0.96	63	73	26	1	98
	55	1.5	1.5	62	74	24	2	97
	65	2.0	2.0	63	70	27	3	97
	75	2.0	2.0	53	72	26	2	97
Ta−SiO_2	35	0.60	0.32	64	47	26	27	40
	45	0.68	0.32	69	49	25	26	27
	55	2.2	0.43	87	48	27	25	21
	65	1.8	0.67	80	56	24	21	35
	75	1.9	0.42	65	54	17	29	27

[a]See standard conditions in text. Yields based on all C6 products detected, relative to limiting H_2O_2. Turnover frequencies (TOF) relative to total metal content. Initial rates through 15 min. [b]Cyclohexenol and cyclohexenone. No cyclohexanone or cyclohexanol observed.

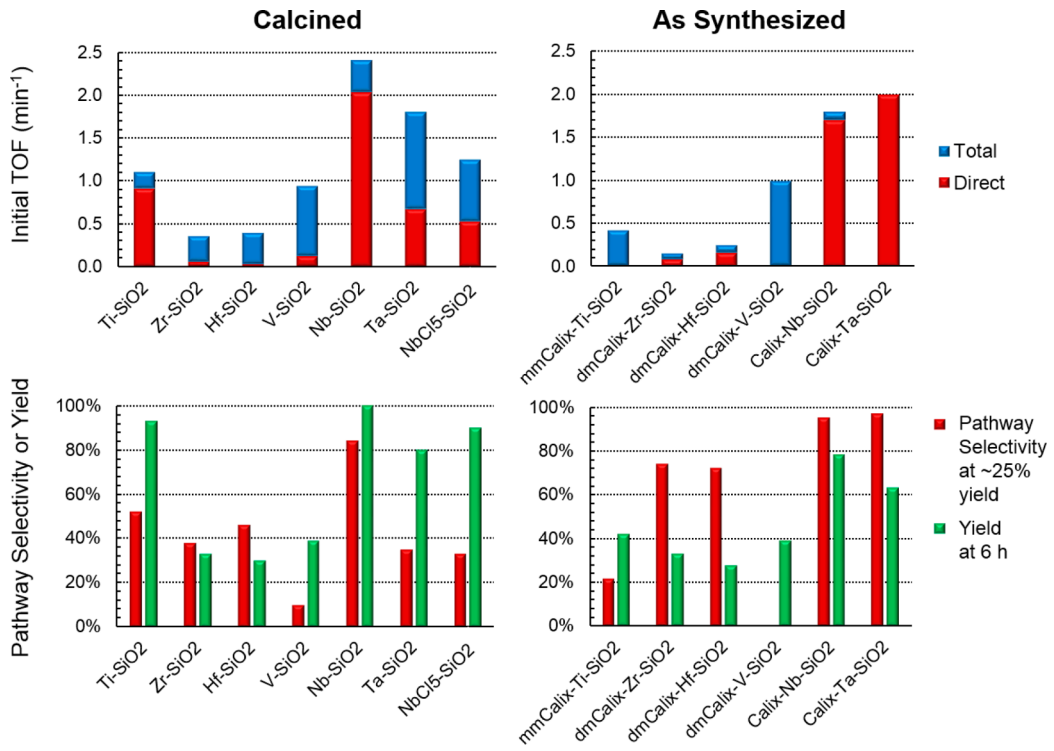

Figure 3. Selected kinetic data for the epoxidation of cyclohexene at 65 °C by groups IV and V calixarene−M−SiO_2 and calcined M−SiO_2. See standard reaction conditions in text. Yields based on all C6 products detected, relative to limiting H_2O_2. Turnover frequencies (TOF) relative to total metal content. Initial rates through 15 min.

epoxide hydrolysis to the *trans*-diol, catalyzed by both Lewis and Brønsted acids, and H_2O_2 decomposition that accounts for the incomplete cyclohexene conversion over most materials.

Accordingly, we use reaction pathway branching selectivity, $R_2/(R_1 + R_2)$ in Scheme 2, as a key metric for assessing catalyst performance. The directly produced epoxide is the sum of epoxide + diol − (cyclohexenol − cyclohexenone), where the latter difference accounts specifically for the cyclohexenol produced during epoxidation by cyclohexenyl hydroperoxide.[21,73,74] The direct pathway selectivity (concisely referred to as *pathway selectivity*) is then the fraction of direct epoxide relative to all C6 products. Grafted calixarene−Ta catalysts were used to find optimal temperatures for further study (Table 3), following prior experience with this system.[21] Both pathway and product selectivities are integrated over the entire product yield to that point, and for most systems studied here, these selectivities change significantly as the reaction proceeds.

Initial rates of epoxidation increase with temperature while product and pathway selectivities at any level of conversion remain largely unchanged with temperature. Generally, Calix−Ta−SiO_2 is a much more selective and active catalyst than calcined Ta−SiO_2, consistent with previous reports by some of us.[21,75] For bare Ta−SiO_2, the highest pathway selectivity was observed at 35 °C, whereas at 75 °C, yields began to suffer, likely due to catalytic decomposition of H_2O_2.

Reaction at 45 and 65 °C offers a balance of high selectivities and fast initial rates, and these temperatures were chosen for kinetic experiments across the periodic series of catalysts. Because initial TOFs across this series span an order of magnitude, here, we also report selectivities at ~25% yield of

DOI: 10.1021/acscatal.5b01105
ACS Catal. 2015, 5, 5077−5088

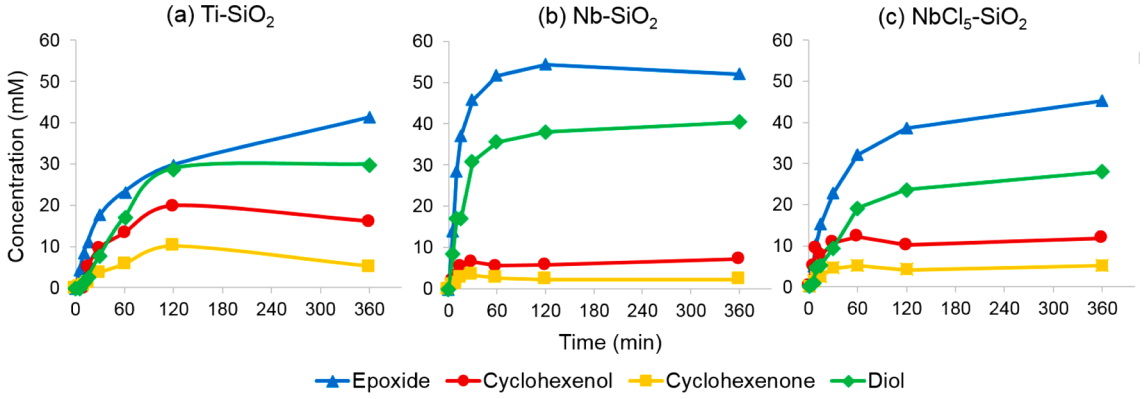

Figure 4. Product yields vs time for cyclohexene oxidation at 65 °C over calcined (a) Ti−SiO_2 and (b) Nb−SiO_2 and (c) the control $NbCl_5$−SiO_2. Note that product yields have the same values when expressed as concentration (mM), percent yield, or turnover numbers.

C6 products as well as the 6-h yield of all C6 products. Figure 3 gives results for the as-synthesized and calcined materials. For a summary of the full results, see Table S2. Selected time-course data are given in Figure 4. For calcined catalysts, the initial reactivity trends Nb > Ta ≫ Ti > V > Hf ∼ Zr, the pathway selectivity at 25% yield trends Nb ≫ Ta ∼ Ti ∼ Hf ∼ Zr ≫ V, and the total 6-h yield trends Nb ∼ Ti > Ta ≫ V > Zr ∼ Hf.

The most striking result is that Nb−SiO_2 derived from the calixarene precursor significantly outperforms all other catalysts, including the common Ti−SiO_2, with respect to rates and pathway selectivity. However, this selectivity and rate advantage disappear for the control Nb catalyst prepared from $NbCl_5$. Zr−SiO_2 and Hf−SiO_2 are signficantly less productive than the other materials and are not significantly different from one another in this and all other metrics. Ta−SiO_2 gives a high total initial rate, but it initially produces significant amounts of radical products, contributing to a low direct rate. Ta−, Ti−, Zr− and Hf−SiO_2 have similar pathway selectivities by the time they reach 25% yield of C6 products. Finally, V−SiO_2 is a poor epoxidation catalyst that proceeds almost exclusively via radical oxidation pathways to give cyclohexenol.[76] For the as-synthesized, calixarene-containing catalysts, the initial reactivity trend is Nb ∼ Ta ≫ V > Ti > Hf ∼ Zr, the trend in pathway selectivity at ∼25% yield is Nb ∼ Ta > Zr ∼ Hf > Ti > V, and the total yield at 6 h trends Nb > Ta > V > Ti > Zr ∼ Hf. Retaining the calixarene ligand significantly improves the pathway selectivity of the second and third row cations in both groups compared with their calcined versions.

All of the high-performing catalysts were tested for potential leaching of active species into solution.[77] For Nb−, Ta−, and Ti−SiO_2, oxidation rates by any leached species were more than an order of magnitude slower than those of the solid (full results in Figures S4−S5 and Table S3), consistent with the observation of negligible leaching by others.[78] Although not active in solution, leached metals cannot be ruled out completely because adding fresh SiO_2 and extra H_2O_2 to the decanted liquid does improve rates relative to the clear solution, suggesting reimmobilization to synthesize new, active species. V−SiO_2 leaches significantly, and homogeneous catalysis appears to contribute substantially to the overall observed reactivity (Figure S5, Table S3), as previously observed by others.[79−81]

Styrene Epoxidation. Styrene's epoxidation reaction network includes overoxidation and isomerization products phenylacetaldehyde, styrene diol, and benzaldehyde (Scheme 3), and the latter is believed to form via oxidative

Scheme 3. Reaction Products in the Catalytic Oxidation of Styrene

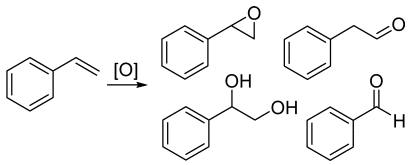

decarboxylation of a transient α-hydroxycarboxylic acid.[82] Epoxidation of the electron-poor styrene is a challenging reaction for d_0 metal oxide catalysts, and yields and epoxide selectivities are correspondingly poorer than for cyclohexene.

For reaction at 65 °C, Figure 5 gives initial rates, epoxide selectivites at ∼10% yield, 6-h selectivites, and total yields. (Full data in Table S4.) After 6 h, all catalysts give <60% epoxide selectivity due to ring opening, isomerization, and other oxidations. For calcined materials, Nb−SiO_2 is again initially the most reactive and selective to epoxide, whereas Hf−SiO_2 and Zr−SiO_2 perform equally poorly. V−SiO_2 is nearly as reactive for styrene as it is for cyclohexene, giving it the highest total yields over 6 h, but again displaying low selectivity to the epoxide. Selectivites change little with reaction progress, indicating that the other products may be predominantly formed in parallel, rather than in sequential pathways. Retaining the calixarene ligand in the as-synthesized catalysts markedly improves the rate for V−SiO_2 and the initial selectivities of Nb−SiO_2 and Ta−SiO_2. The selectivities of these latter two catalysts decrease significantly with reaction progress, consistent with the formation of the other oxygenates as secondary products. This indicates that the ligand specifically enhances the rate to the epoxide.

Oxide Structure and Stability. XANES was used to further understand surface speciation and local coordination geometry for Ti[9,14,53] and Nb[39] catalysts before and after use. These metal oxides display distinct pre-edge features from 1s to 3d transitions that allow for fingerprinting of the metal−oxygen coordination environment by comparison with oxide standards of known coordination number.[83] The intensity and position of pre-edge peaks from Ti-containing materials were correlated to average Ti−O coordination numbers using Ba_2TiO_4 (4-coordinate), $Ba_2(TiO)Si_2O_7$ Fresnoite (5-coordinate), and TiO_2 anatase (6-coordinate) standards (Figure S6).[42,84−86] Similarly, the pre-edge intensity in Nb-containing materials was correlated to average Nb−O coordination numbers using $YNbO_4$ (4-coordinate),[51] $CaNb_2O_6$ (5-coordinate),[52,87] and

DOI: 10.1021/acscatal.5b01105
ACS Catal. 2015, 5, 5077−5088

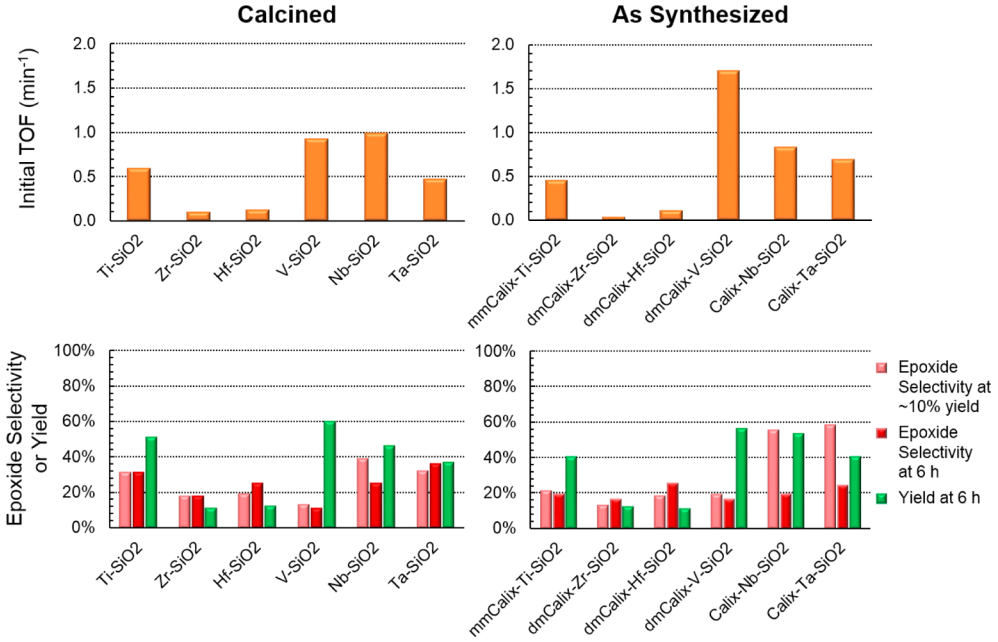

Figure 5. Selected kinetic data for the epoxidation of styrene at 65 °C by groups IV and V calixarene−M−SiO_2 and calcined M−SiO_2. See standard reaction conditions in text. Yields based on detected epoxide, diol, phenylacetaldehyde, and benzaldehyde relative to limiting H_2O_2. Turnover frequencies (TOF) relative to total metal content. Initial rates through 15 min.

$KNbO_3$ (6-coordinate) standards (Figures 6, S7). Nb_2O_5 is also octahedral, but exhibits first-coordination disorder, giving it a lower pre-edge feature height. For discussion purposes, the experimental catalysts are assigned a coordination number on the basis of correlations to these materials as follows (Table 4): For the Nb-containing catalysts, pre-edge peak heights of 0.19−0.15 indicate coordination numbers between 4 and 5 or disordered 4-coordinate structures. Values of 0.15−0.12 indicate coordination numbers between 5 and 6 or disordered 5-coordinate structures. Values below 0.12 indicate disordered 6-coordinate structures.

Three conclusions are made by the fits to the fresh catalysts. First, the calixarene ligand is clearly attached to the metal sites, as it increases in coordination number (C.N.) or disorder for both Nb and Ti, relative to the calcined catalysts. Second, the Nb−SiO_2 derived from calixarene is much more under-coordinated than the analogous control catalyst derived from $NbCl_5$, consistent with its lower optical edge and catalyst proficency. Finally, the calcined Ti−SiO_2 and Nb−SiO_2 catalysts have nearly identical effective C.N. Overall, these results demonstrate that the ligand enforces a similar—and similarly undercoordinated—environment at the active metal.

Following use in epoxidation, the C.N. of Nb−SiO_2 increases from 4.5 to 5.9, whereas Ti−SiO_2 maintains its mostly tetrahedral coordination environment. However, recalcination of spent Nb−SiO_2 recovers the pre-edge feature of the fresh material, indicating that the catalyst strongly adsorbs species from the reaction mixture rather than being irreversibly deactivated through oxide aggregation. Others have recently noted negligible restructuring in NbO_x−SiO_2 catalysts for limonene epoxidation.[78] DRUV−vis spectra mirror these changes (Figure S8), with the optical edge of Nb−SiO_2 decreasing from 4.0 to 3.0 eV after use and washing but recovering to 3.7 eV after recalcination. In accordance with these spectral changes, the recovered Nb−SiO_2 catalyst is poorly active after simple washing, but recovers ∼90% of its activity after a recalcination. In contrast, DRUV−vis spectra of recovered Ta−SiO_2 indicate severe restructuring upon recalcination (Figure S9).

Finally, it must be noted that the as-synthesized Calix−Nb−SiO_2 is not particularly robust: the DRUV−vis (Figure S8) suggests the ligand is largely lost during reaction or washing, also consistent with an increase in the XANES pre-edge intensity after use and washing, and the known tendency for ligand loss during synthesis. Although some of us have seen mmCalix−Ti−SiO_2 and Calix−Ta−SiO_2 appear to be quite stable in prior studies,[21,40] it is recommended to calcine the freshly prepared Calix−Nb−SiO_2 in the interest of stability.

DISCUSSION

The reactivity data set is examined in several ways to draw larger conclusions. First, Figure 7 plots pathway selectivity vs yield of oxygenates in cyclohexene oxidation. Ti−, Ta−, and Nb−SiO_2 are all able to reach >80% yield of oxygenates, whereas Zr- and Hf-containing catalysts give poor yields, even over long times. V−SiO_2, which is selective to the radical pathway, gives the worst yields because it utilizes oxidant less efficiently.[21,75] It should also be emphasized that Figure 7 plots the integrated *pathway* selectivity, not the net selectivity to epoxide, which is given in Table S2. The most active catalysts for epoxidation do also have a high rate of epoxide hydrolysis.

Figure 7a illustrates three main modes of reactivity within this catalyst family: (1) calixarene-derived Nb−SiO_2, which uniquely maintains high pathway selectivity (∼85%) across all yields; (2) V−SiO_2, which is always poorly selective (<20%); and (3) all other catalysts, including $NbCl_5$−SiO_2, which suffer from early stage (<10% yield) low pathway selectivities that improve at higher conversions. We note again that Figure 7 plots selectivities integrated over the entire product yield to that point; thus, the upward trend in pathway selectivity (dotted curve) is a consequence of the system's poorly selectivity at low conversion (i.e., large initial production of

DOI: 10.1021/acscatal.5b01105
ACS Catal. 2015, 5, 5077−5088

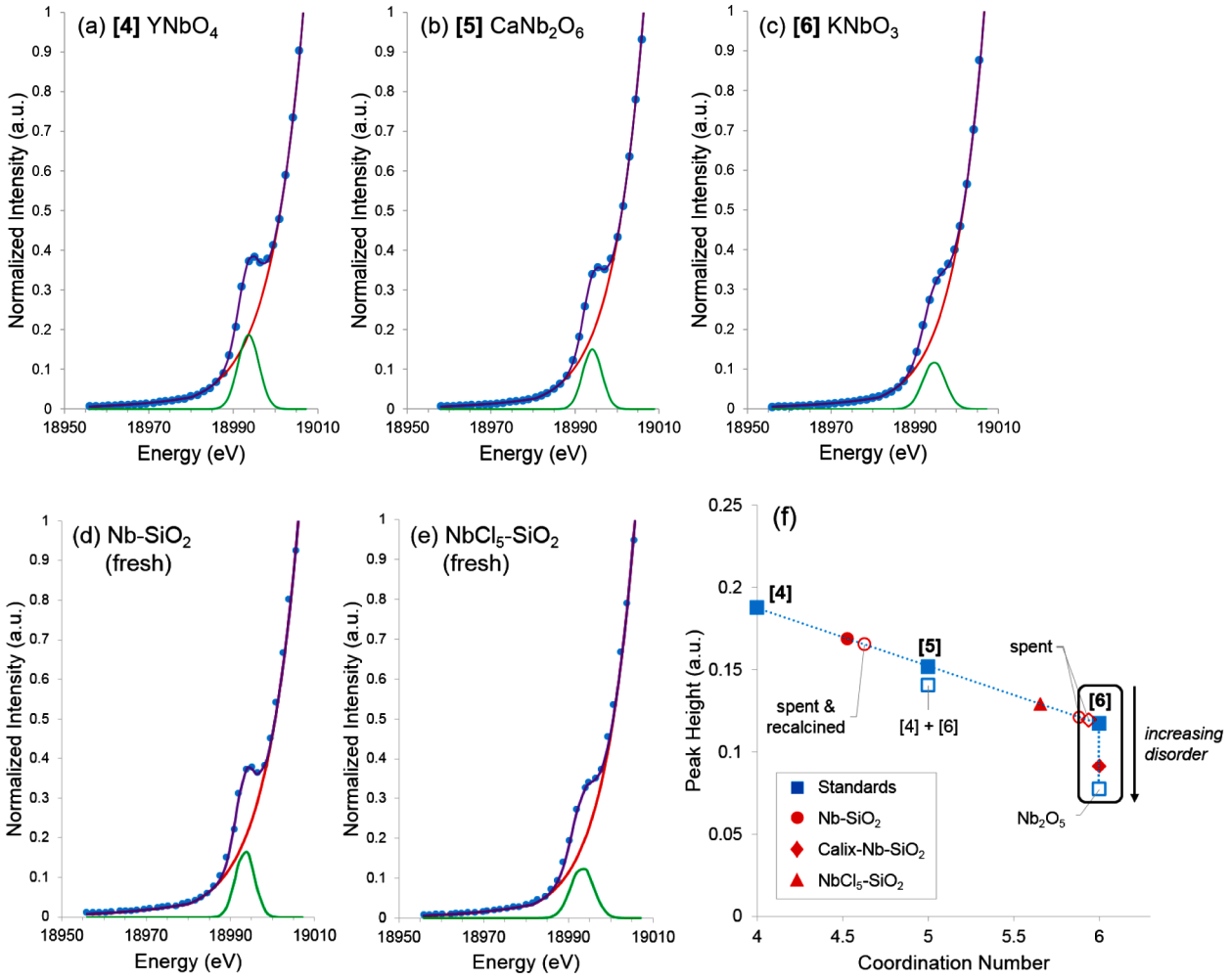

Figure 6. Nb K-edge XANES and fitting of pre-edge feature for (a) 4-coordinate $YNbO_4$, (b) 5-coordinate $CaNb_2O_6$, (c) 6-coordinate $KNbO_3$, (d) $Nb-SiO_2$, and (e) $NbCl_5-SiO_2$. Fitting details are in Experimental Methods and the SI. (f) Linear correlation between pre-edge feature intensity and coordination number of standards, then used to interpolate values for the experimental materials $Nb-SiO_2$, $Calix-Nb-SiO_2$, and $NbCl_5-SiO_2$.

Table 4. XANES Summary for Ti and Nb Catalysts

		pre-edge[a]		
catalyst	condition	energy (eV)	sharpness[b]	C.N.
$mmCalix-Ti-SiO_2$	fresh	4970.6	0.77	4.8
	spent[c]	4970.9	0.66	5.4
$Ti-SiO_2$	fresh	4970.0	0.88	4.4
	spent[c]	4970.1	0.89	4.4
$Calix-Nb-SiO_2$	fresh	18 993	0.09	6.0[e]
	spent[c]	18 994	0.12	5.9
$Nb-SiO_2$	fresh	18 993	0.17	4.5
	spent[c]	18 994	0.12	5.9
	recalcined[d]	18 994	0.17	4.6
$NbCl_5-SiO_2$	fresh	18 993	0.13	5.6

[a]See Figures S6 (Ti), 6, and S7 (Nb) for pre-edge fitting and correlations between fitted features and coordination number (C.N.). [b]For Ti: sharpness parameter $(A_2 + A_3)/A_{TOT}$, see Figure S6. For Nb: peak intensity. [c]Following 6 h of cyclohexene epoxidation at 65 °C, standard conditions. Solids were vacuum-filtered, washed with excess acetonitrile, and dried at 150 °C under dynamic vacuum for 2 h. [d]Treated as in footnote c with subsequent calcination in air at 550 °C for 6 h. [e]Substantially disordered.

radical products), followed by a pronounced switch to high pathway selectivity as the reaction proceeds.

Figure 7b shows that retaining the calixarene ligand enhances the pathway selectivity of the second and third row cations relative to their calcined analogues at all levels of conversion. In particular, $Calix-Ta-SiO_2$ is remarkably selective compared with its calcined version, which is consistent with earlier observations by some of us.[21] The ligand has a weaker effect on Ti and V.

A unifying hypothesis is that aggregates of MO_x, as distinguished from isolated M cations, are responsible for the observed initial radical reactivity. DRUV–vis (Figure 2b) and XANES (Figure 6) show the $Nb-SiO_2$ to be undercoordinated relative to $NbCl_5$-derived catalysts, and DRUV–vis indicates the presence of some larger aggregates in $Ta-SiO_2$ (Figure 2b). All these latter catalysts initially show the radical pathway. Further, the presence of coordinated calixarene will help minimize MO_x formation under reaction conditions, boosting pathway selectivity in nearly all cases. Application of chemical titration techniques recently developed by our group[88] is currently underway to address these unique behaviors and others.

For the calcined catalysts, we further compare reactivity patterns with the ionic character of the metal–oxygen bond at

DOI: 10.1021/acscatal.5b01105
ACS Catal. 2015, 5, 5077–5088

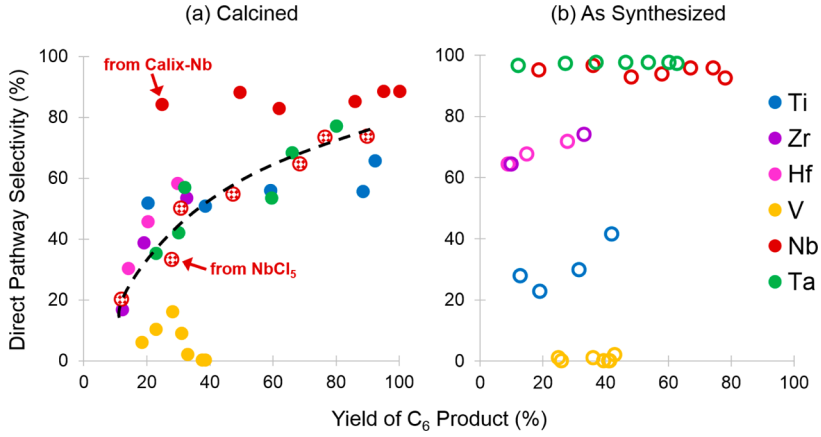

Figure 7. Integrated selectivity toward direct oxidation pathways vs total yield of C6 product for cyclohexene oxidation at 65 °C by (a) calcined catalysts (solid circles) and (b) calixarene-containing catalysts (open circles). Calculated selectivities at less than ~10% yield are unreliable and have been removed from comparison.

the SiO_2 surface using the Pauling scale of electronegativity (Figure 8). Here, we approximate ionic character by subtracting

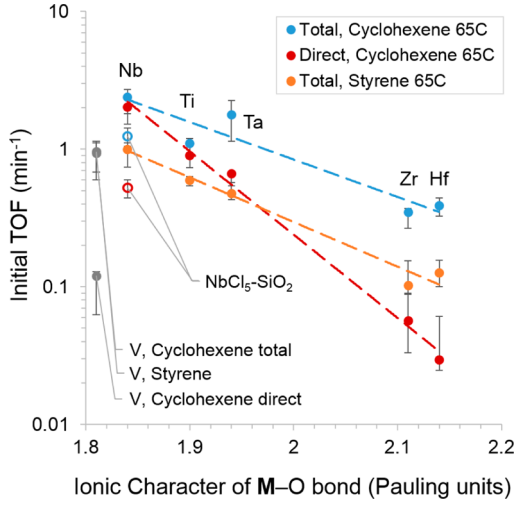

Figure 8. Correlations between oxidation TOFs (min^{-1}) with ionic character of the M−O bond for calcined catalysts. Ionic character is estimated by subtracting the Pauling electronegativity of each metal from that of oxygen.[89] Error bars represent alternative calculations of TOF from 10 min (high) and 30 min (low) of reaction. Redox-active V−SiO_2 has been excluded from comparison.

each metal's Pauling electronegativity[89] from that of oxygen (i.e., $\chi_O - \chi_M$) and correlate this metric with our calculated initial turnover frequencies. Alternately, the following conclusions hold if the stoichiometry of an assumed MO_4 monomer is geometrically averaged for the electronegativity metric (i.e., by calculating $[(\chi_M)\cdot(\chi_O)^4]^{1/5}$; see Figure S10).

Initial, direct TOF for cyclohexene is both strongly sensitive to and tightly correlated with decreasing ionic character over a nearly 100-fold change in rate, suggesting that this reaction is a readout of intrinsic Lewis acidity. Others have strongly correlated atomic electronegativity with Lewis acid strength for main-group elements in their highest oxidation state,[90] as well as for lanthanide(III) complexes.[89,91] The total TOF for styrene also correlates strongly with ionic character but is less sensitive. Interestingly, the relative intensity of the calixarene phenolate LMCT in the DRUV−vis spectra of Figure 2a varies dramatically across different metals and in the same order as epoxidation reactivity and ionic character, again with the exception of V. This trend suggests that the relative intensity of this feature is sensitive to the strength of ligand binding and itself is a proxy for reactivity in Lewis acid catalysis.

Finally, the total TOF for cyclohexene (i.e., including radical products) is less strongly predictive of Lewis activity, confounded by the kinetically coupled pathways. V−SiO_2 has been excluded from these comparisons because it appears to proceed by a distinct redox mechanism and due to observations of leaching.[4,30] According to this calculation, Nb is an intrinsically good catalyst for electrophilic activation of H_2O_2 because it can be synthesized in a stable, highly undercoordinated state, is strongly covalent, and is practically redox-inactive under these conditions. Beyond high activity for electrophilic activation of H_2O_2, the Nb−SiO_2 synthesized from the calixarene precursor is also uniquely pathway-selective within this series, giving <15% radical pathway selectivity at all conversions. Crucially, the rates and pathway selectivities of the conventionally synthesized $NbCl_5$−SiO_2 do not fit along these trends, further demonstrating the importance of the calixarene platform for controlling the oxide structure and enabling this systematic study.

CONCLUSIONS

Catalysts for styrene and cyclohexene epoxidation with H_2O_2 were synthesized by grafting calixarene complexes of Ti(IV), Zr(IV), Hf(IV), V(V), Nb(V), and Ta(V) (all of groups IV and V) to SiO_2 at surface densities 0.22 ± 0.03 M nm^{-2}. Typically, different supported metal oxides are synthesized in separate investigations and by a range of techniques, resulting in a range of supported oxide structures. This structural diversity can make it difficult to compare reactivities and selectivities across related metal oxides. Here, the systematic use of a single type of precursor reveals a 100-fold change in Lewis acid-catalyzed direct cyclohexene epoxidation rates, which correlate well with the ionic bond character of the supported oxide. V−SiO_2 is an exception that appears to follow a distinct mechanism. This trend is observed only when the calixarene ligand is used in the precursor synthesis; Nb−SiO_2 from $NbCl_5$ is much less reactive and selective. DRUV−vis and XANES indicate that systematic use of the calixarene complex in synthesis helps keep the final, calcined catalyst highly dispersed, improving reactivity and allowing comparisons among structurally similar sites. Even for

DOI: 10.1021/acscatal.5b01105
ACS Catal. 2015, 5, 5077−5088

Ta−SiO_2, in which some aggregated TaO_x is evidenced from the DRUV−vis, its agreement with the correlation of Figure 8 indicates that the vast majority of the Ta sites are active, isolated sites. Finally, the as-synthesized catalysts (with the ligand retained) have markedly higher direct pathway selectivities for the second and third row transition metal oxides, again presumably because the ligand helps keep the individual cations isolated from one another.

Throughout this study, the calcined Nb−SiO_2 derived from the calixarene precursor is high-performing, with an initial TOF in cyclohexene epoxidation (2.4 min^{-1}) >2 times faster than a more standard Ti−SiO_2. Further, all materials except this Nb−SiO_2 exhibit an initial period of radical oxidation before switching to direct pathways as the reaction proceeds. This gives the Nb−SiO_2 an exceptional pathway selectivity of ∼85% over the entire course of the reaction. Finally, calcined Nb−SiO_2 is stable to leaching and maintains activity and pathway selectivity upon regeneration and reuse. Overall, NbO_x−SiO_2 materials have received much less attention as selective oxidation catalysts,[78,92,93] in contrast with extensive work on Ti−SiO_2. This includes supported[22,25,26] and co-condensed[23,94,95] NbO_x−SiO_2 catalysts that have been demonstrated by others as highly active and selective for alkene epoxidation. These results highlight supported Nb−SiO_2 as a highly active and pathway-selective catalyst for these transformations. This conclusion is reached only when it is synthesized utilizing bulky precursors, such as the calixarene complex, that enable and enforce high dispersion of the oxide. Additional studies on these high-performing Nb−SiO_2 catalysts are underway.

■ ASSOCIATED CONTENT

Supporting Information

The Supporting Information is available free of charge on the ACS Publications website at DOI: 10.1021/acscatal.5b01105.

Detailed synthetic procedures, NMR resonances and elemental analyses for calixarene complexes and grafted catalysts; synthesis procedures and powder X-ray diffraction spectra of X-ray absorption standards $YNbO_4$ and $CaNb_2O_6$; full kinetic data for cyclohexene and styrene epoxidation at 45 and 65 °C; cyclohexene epoxidation (65 °C) leaching (Ti, V, Nb, Ta) and recycle (Nb) experiments; additional characterization (UV−vis, ^{13}C NMR) for calixarene complexes of Ti, Zr, Hf, V, Nb, and Ta; X-ray absorption spectroscopy E_0 (eV) for Ti, V, Nb and Ta; Gaussian peak fitting for Ti and Nb pre-edge XANES features; DRUV−vis spectroscopy of recovered Nb−SiO_2, calix−Nb−SiO_2 and Ta−SiO_2; and an alternate correlation between oxidation TOF and ionic character of assumed MO_4 oxide monomers (PDF)

■ AUTHOR INFORMATION

Corresponding Author

*E-mail: j-notestein@northwestern.edu.

Notes

The authors declare no competing financial interest.

■ ACKNOWLEDGMENTS

N.E.T. and J.M.N. acknowledge financial support from the Dow Chemical Company. A.B.T. acknowledges financial support from NSF Grant CBET-0933667. Characterization was performed at IMSERC at Northwestern University with the support of NSF Grant DMR-0521267 and at the DuPont−Northwestern−Dow Collaborative Access Team (DND-CAT) at the Advanced Photon Source at Argonne National Laboratory (DOE Contract No. DE-AC02-06CH11357). N.E.T. thanks Dr. Qing Ma for his assistance with X-ray absorption spectroscopy experiments. Powder X-ray diffraction experiments were performed at the J. B. Cohen X-ray Diffraction Facility supported by the MRSEC program of the National Science Foundation (DMR-1121262) at the Materials Research Center of Northwestern University.

■ REFERENCES

(1) Bartholomew, C. H.; Farrauto, R. J. *Fundamentals of Industrial Catalytic Processes*, 2nd ed.; Wiley: Hoboken, NJ, 2006.
(2) Clerici, M. G.; Kholdeeva, O. A. *Liquid Phase Oxidation via Heterogeneous Catalysis: Organic Synthesis and Industrial Applications*; Wiley: Hoboken, NJ, 2013.
(3) Thomas, J. M.; Thomas, W. J. *Principles and Practice of Heterogeneous Catalysis*; Wiley VCH: New York, NY, 2005.
(4) Sheldon, R. A. *J. Mol. Catal.* **1980**, *7*, 107−126.
(5) Thomas, J. M.; Raja, R.; Lewis, D. W. *Angew. Chem., Int. Ed.* **2005**, *44*, 6456−82.
(6) Clerici, M. G.; Bellussi, G.; Romano, U. *J. Catal.* **1991**, *129*, 159−167.
(7) Clerici, M. G.; Ingallina, P. *J. Catal.* **1993**, *140*, 71−83.
(8) Gao, X.; Wachs, I. E. *Catal. Today* **1999**, *51*, 233−254.
(9) Capel-Sanchez, M. C.; Blanco-Brieva, G.; Campos-Martin, J. M.; de Frutos, M. P.; Wen, W.; Rodriguez, J. A.; Fierro, J. L. G. *Langmuir* **2009**, *25*, 7148−7155.
(10) Marchese, L.; Gianotti, E.; Dellarocca, V.; Maschmeyer, T.; Rey, F.; Coluccia, S.; Thomas, J. M. *Phys. Chem. Chem. Phys.* **1999**, *1*, 585−592.
(11) Gianotti, E.; Bisio, C.; Marchese, L.; Guidotti, M.; Ravasio, N.; Psaro, R.; Coluccia, S. *J. Phys. Chem. C* **2007**, *111*, 5083−5089.
(12) Ratnasamy, P.; Srinivas, D.; Knözinger, H. *Adv. Catal.* **2004**, *48*, 1−169.
(13) Notari, B.; Willey, R. J.; Panizza, M.; Busca, G. *Catal. Today* **2006**, *116*, 99−110.
(14) Gao, X.; Bare, S. R.; Fierro, J. L. G.; Banares, M. A.; Wachs, I. E. *J. Phys. Chem. B* **1998**, *102*, 5653−5666.
(15) Maschmeyer, T.; Rey, F.; Sankar, G.; Thomas, J. M. *Nature* **1995**, *378*, 159−162.
(16) Copéret, C.; Chabanas, M.; Petroff Saint-Arroman, R.; Basset, J.-M. *Angew. Chem., Int. Ed.* **2003**, *42*, 156−181.
(17) Jarupatrakorn, J.; Tilley, T. D. *J. Am. Chem. Soc.* **2002**, *124*, 8380−8388.
(18) Meunier, D.; de Mallmann, A.; Basset, J.-M. *Top. Catal.* **2003**, *23*, 183−189.
(19) Brutchey, R. L.; Lugmair, C. G.; Schebaum, L. O.; Tilley, T. D. *J. Catal.* **2005**, *229*, 72−81.
(20) Ruddy, D. A.; Tilley, T. D. *J. Am. Chem. Soc.* **2008**, *130*, 11088−11096.
(21) Morlanés, N.; Notestein, J. M. *J. Catal.* **2010**, *275*, 191−201.
(22) Nowak, I.; Kilos, B.; Ziolek, M.; Lewandowska, A. *Catal. Today* **2003**, *78*, 487−498.
(23) Kilos, B.; Nowak, I.; Ziolek, M.; Tuel, A.; Volta, J. C. *Stud. Surf. Sci. Catal. B* **2005**, *158*, 1461−1468.
(24) Trejda, M.; Tuel, A.; Kujawa, J.; Kilos, B.; Ziolek, M. *Microporous Mesoporous Mater.* **2008**, *110*, 271−278.
(25) Gallo, A.; Tiozzo, C.; Psaro, R.; Carniato, F.; Guidotti, M. *J. Catal.* **2013**, *298*, 77−83.
(26) Tiozzo, C.; Bisio, C.; Carniato, F.; Gallo, A.; Scott, S. L.; Psaro, R.; Guidotti, M. *Phys. Chem. Chem. Phys.* **2013**, *15*, 13354−62.
(27) Tiozzo, C.; Bisio, C.; Carniato, F.; Marchese, L.; Gallo, A.; Ravasio, N.; Psaro, R.; Guidotti, M. *Eur. J. Lipid Sci. Technol.* **2013**, *115*, 86−93.
(28) Weckhuysen, B. M.; Keller, D. E. *Catal. Today* **2003**, *78*, 25−46.
(29) Mars, P.; van Krevelen, D. W. *Chem. Eng. Sci.* **1954**, *3*, 41−59.

DOI: 10.1021/acscatal.5b01105
ACS Catal. 2015, 5, 5077−5088

(30) Sheldon, R. A.; Van Doorn, J. A. *J. Catal.* **1973**, *31*, 427−437.
(31) Sheldon, R. *Bull. Soc. Chim. Belg.* **1985**, *94*, 651−670.
(32) Corma, A.; Iborra, S.; Mifsud, M.; Renz, M. *J. Catal.* **2005**, *234*, 96−100.
(33) Boronat, M.; Corma, A.; Renz, M.; Viruela, P. M. *Chem.—Eur. J.* **2006**, *12*, 7067−7077.
(34) Kholdeeva, O. A.; Maksimovskaya, R. I. *J. Mol. Catal. A: Chem.* **2007**, *262*, 7−24.
(35) Joergensen, K. A. *Chem. Rev.* **1989**, *89*, 431−458.
(36) Li, Z.; Yamamoto, H. *J. Am. Chem. Soc.* **2010**, *132*, 7878−7880.
(37) Aoto, H.; Matsui, K.; Sakai, Y.; Kuchizi, T.; Sekiya, H.; Osada, H.; Yoshida, T.; Matsunaga, S.; Nomiya, K. *J. Mol. Catal. A: Chem.* **2014**, *394*, 224−231.
(38) Wegener, S. L.; Marks, T. J.; Stair, P. C. *Acc. Chem. Res.* **2012**, *45*, 206−214.
(39) Jehng, J. M.; Wachs, I. E. *J. Phys. Chem.* **1991**, *95*, 7373−7379.
(40) Notestein, J. M.; Iglesia, E.; Katz, A. *J. Am. Chem. Soc.* **2004**, *126*, 16478−16486.
(41) Notestein, J. M.; Andrini, L. R.; Requejo, F. G.; Katz, A.; Iglesia, E. *J. Am. Chem. Soc.* **2007**, *129*, 15585−15595.
(42) Notestein, J. M.; Andrini, L. R.; Kalchenko, V. I.; Requejo, F. G.; Katz, A.; Iglesia, E. *J. Am. Chem. Soc.* **2007**, *129*, 1122−1131.
(43) Wang, W.-G.; Zheng, Q.-Y.; Huang, Z.-T. *Synth. Commun.* **1999**, *29*, 3711−3718.
(44) Zanotti-Gerosa, A.; Solari, E.; Giannini, L.; Floriani, C.; Re, N.; Chiesi-Villa, A.; Rizzoli, C. *Inorg. Chim. Acta* **1998**, *270*, 298−311.
(45) Caselli, A.; Solari, E.; Scopelliti, R.; Floriani, C.; Re, N.; Rizzoli, C.; Chiesi-Villa, A. *J. Am. Chem. Soc.* **2000**, *122*, 3652−3670.
(46) Castellano, B.; Solari, E.; Floriani, C.; Re, N.; Chiesi-Villa, A.; Rizzoli, C. *Chem.—Eur. J.* **1999**, *5*, 722−737.
(47) Giannini, L.; Solari, E.; Zanotti-Gerosa, A.; Floriani, C.; Chiesi-Villa, A.; Rizzoli, C. *Angew. Chem., Int. Ed. Engl.* **1996**, *35*, 85−87.
(48) Castellano, B.; Solari, E.; Floriani, C.; Re, N.; Chiesi-Villa, A.; Rizzoli, C. *Organometallics* **1998**, *17*, 2328−2336.
(49) de Silva, N.; Hwang, S.-J.; Durkin, K. A.; Katz, A. *Chem. Mater.* **2009**, *21*, 1852−1860.
(50) Bland, J. *Acta Crystallogr.* **1961**, *14*, 875−881.
(51) Mather, S. A.; Davies, P. K. *J. Am. Ceram. Soc.* **1995**, *78*, 2737−2745.
(52) Lapina, O. B.; Khabibulin, D. F.; Romanenko, K. V.; Gan, Z.; Zuev, M. G.; Krasil'nikov, V. N.; Fedorov, V. E. *Solid State Nucl. Magn. Reson.* **2005**, *28*, 204−224.
(53) Thomas, J. M.; Sankar, G. *Acc. Chem. Res.* **2001**, *34*, 571−581.
(54) Yoshida, S.; Tanaka, T.; Hanada, T.; Hiraiwa, T.; Kanai, H.; Funabiki, T. *Catal. Lett.* **1992**, *12*, 277−285.
(55) Jehng, J.-M.; Hu, H.; Gao, X.; Wachs, I. E. *Catal. Today* **1996**, *28*, 335−350.
(56) Yoshida, S.; Nishimura, Y.; Tanaka, T.; Kanai, H.; Funabiki, T. *Catal. Today* **1990**, *8*, 67−75.
(57) Piilonen, P. C.; Farges, F.; Linnen, R. L.; Brown, G. E.; Pawlak, M.; Pratt, A. *Can. Mineral.* **2006**, *44*, 775−794.
(58) Tanaka, T.; Yoshida, T.; Yoshida, H.; Aritani, H.; Funabiki, T.; Yoshida, S.; Jehng, J.-M.; Wachs, I. E. *Catal. Today* **1996**, *28*, 71−78.
(59) Tanaka, T.; Nojima, H.; Yamamoto, T.; Takenaka, S.; Funabiki, T.; Yoshida, S. *Phys. Chem. Chem. Phys.* **1999**, *1*, 5235−5239.
(60) Nemana, S.; Sun, J.; Gates, B. C. *J. Phys. Chem. C* **2008**, *112*, 7477−7485.
(61) Wieser, C.; Dieleman, C. B.; Matt, D. *Coord. Chem. Rev.* **1997**, *165*, 93−161.
(62) Floriani, C.; Floriani-Moro, R. *Adv. Organomet. Chem.* **2001**, *47*, 167−233.
(63) Homden, D. M.; Redshaw, C. *Chem. Rev.* **2008**, *108*, 5086−5130.
(64) Barton, D. G.; Shtein, M.; Wilson, R. D.; Soled, S. L.; Iglesia, E. *J. Phys. Chem. B* **1999**, *103*, 630−640.
(65) Argyle, M. D.; Chen, K.; Resini, C.; Krebs, C.; Bell, A. T.; Iglesia, E. *J. Phys. Chem. B* **2004**, *108*, 2345−2353.
(66) Modén, B.; Oliviero, L.; Dakka, J.; Santiesteban, J. G.; Iglesia, E. *J. Phys. Chem. B* **2004**, *108*, 5552−5563.
(67) Prieto-Centurion, D.; Boston, A. M.; Notestein, J. M. *J. Catal.* **2012**, *296*, 77−85.
(68) Tauc, J.; Menth, A. *J. Non-Cryst. Solids* **1972**, *8−10*, 569−585.
(69) Lewis, J. D.; Van de Vyver, S.; Crisci, A. J.; Gunther, W. R.; Michaelis, V. K.; Griffin, R. G.; Román-Leshkov, Y. *ChemSusChem* **2014**, *7*, 2255−2265.
(70) Gao, X.; Wachs, I. E. *J. Phys. Chem. B* **2000**, *104*, 1261−1268.
(71) Young, P. D.; Notestein, J. M. *ChemSusChem* **2011**, *4*, 1671−8.
(72) Carniti, P.; Gervasini, A.; Marzo, M. *J. Phys. Chem. C* **2008**, *112*, 14064−14074.
(73) Fraile, J. M.; García, J. I.; Mayoral, J. A.; Vispe, E. *Appl. Catal., A* **2003**, *245*, 363−376.
(74) Fraile, J.; Garcia, J.; Mayoral, J.; Vispe, E. *J. Catal.* **2005**, *233*, 90−99.
(75) Morlanés, N.; Notestein, J. M. *Appl. Catal., A* **2010**, *387*, 45−54.
(76) Rigutto, M. S.; van Bekkum, H. *J. Mol. Catal.* **1993**, *81*, 77−98.
(77) Sheldon, R. A.; Wallau, M.; Arends, I. W. C. E.; Schuchardt, U. *Acc. Chem. Res.* **1998**, *31*, 485−493.
(78) Tiozzo, C.; Palumbo, C.; Psaro, R.; Bisio, C.; Carniato, F.; Gervasini, A.; Carniti, P.; Guidotti, M. *Inorg. Chim. Acta* **2015**, *431*, 190−196.
(79) Deng, Y.; Lettmann, C.; Maier, W. F. *Appl. Catal., A* **2001**, *214*, 31−46.
(80) Carvalho, W. A.; Varaldo, P. B.; Wallau, M.; Schuchardt, U. *Zeolites* **1997**, *18*, 408−416.
(81) Sudhakar Reddy, J.; Liu, P.; Sayari, A. *Appl. Catal., A* **1996**, *148*, 7−21.
(82) Feng, Q.; Song, Q. *J. Org. Chem.* **2014**, *79*, 1867−71.
(83) Yamamoto, T. *X-Ray Spectrom.* **2008**, *37*, 572−584.
(84) Farges, F.; Brown, G. E.; Rehr, J. J. *Phys. Rev. B: Condens. Matter Mater. Phys.* **1997**, *56*, 1809−1819.
(85) Grunes, L. A. *Phys. Rev. B: Condens. Matter Mater. Phys.* **1983**, *27*, 2111−2131.
(86) Eaton, T. R.; Campos, M. P.; Gray, K. A.; Notestein, J. M. *J. Catal.* **2014**, *309*, 156−165.
(87) Cummings, J. P.; Simonsen, S. F. *Am. Mineral.* **1970**, *55*, 90−97.
(88) Eaton, T. R.; Boston, A. M.; Thompson, A. B.; Gray, K. A.; Notestein, J. M. *ChemCatChem* **2014**, *6*, 3215−3222.
(89) Li, K.; Xue, D. *Chin. Sci. Bull.* **2009**, *54*, 328−334.
(90) Brown, I. D.; Skowron, A. *J. Am. Chem. Soc.* **1990**, *112*, 3401−3403.
(91) Tsuruta, H.; Yamaguchi, K.; Imamoto, T. *Tetrahedron* **2003**, *59*, 10419−10438.
(92) Tanabe, K. *Catal. Today* **1990**, *8*, 1−11.
(93) Nowak, I.; Ziolek, M. *Chem. Rev.* **1999**, *99*, 3603−3624.
(94) Ziolek, M.; Nowak, I. *Zeolites* **1997**, *18*, 356−360.
(95) Somma, F.; Canton, P.; Strukul, G. *J. Catal.* **2005**, *229*, 490−498.

DOI: 10.1021/acscatal.5b01105
ACS Catal. 2015, 5, 5077−5088